Radiative lifetimes of the (1–3) $^1\Pi$ states in NaCs: Experiment and theory

I. Klincare, J. Zaharova, M. Tamanis, and R. Ferber
Department of Physics and Institute of Atomic Physics and Spectroscopy, University of Latvia, Rainis Boulevard 19, LV-1586 Riga, Latvia

A. Zaitsevskii, E. A. Pazyuk, and A. V. Stolyarov
Department of Chemistry, Moscow State University, Moscow, 119992, Russia
(Received 20 April 2007; published 28 September 2007)

The radiative lifetimes of the (3) $^1\Pi$ and $D(2)$ $^1\Pi$ states of the NaCs molecule have been directly measured in a thermal cell from fluorescence kinetics after modulated laser excitation. The experimental $\tau^{\mathrm{rad}}_{(3)\,^1\Pi}$ values of the (3) $^1\Pi(v' \in [3,25]; J' \in [25,106])$ levels decrease from 29 to 21 ns as the v' values increase. The measured $\tau^{\mathrm{rad}}_{(3)\,^1\Pi}$ values for two rotational $J'=45$ and 106 levels of the $v'=3$ state are 29 and 25 ns, respectively, showing the effect of rotation. The experimental $\tau^{\mathrm{rad}}_{(2)\,^1\Pi}$ value of the $D(2)$ $^1\Pi(v'=0; J'=16)$ level is about 37 ns. The average measured effective quenching collision cross section of excited NaCs molecule with Cs atoms $\sigma=(3.5\pm1.5)\times10^{-14}$ cm^2. The theoretical radiative lifetimes for the lowest (1–3) $^1\Pi$ states have been evaluated in the framework of a pure **a** Hund's coupling case using the approximate sum rule over the lower-lying vibronic states. The required quasirelativistic transition dipole moments were calculated by many-body multipartitioning theory. Propagation of the systematic errors of *ab initio* transition moments and potential energy curves (PECs) into the τ^{rad} values is discussed. The best lifetime estimates predicted for particular rovibronic levels of the (3) $^1\Pi$ and $D(2)$ $^1\Pi$ states agree with their experimental counterparts within 2–8 % which can be compared with the 1–3 % uncertainties in the measured τ^{expt} values. The lifetimes of the $B(1)$ $^1\Pi$ and (3) $^1\Pi$ states are almost exclusively determined by a single transition to the ground X $^1\Sigma^+$ state while a contribution of the $D(2)$ $^1\Pi \rightarrow A$ $^1\Sigma^+$ transition into the $\tau^{\mathrm{rad}}_{(2)\,^1\Pi}$ values reaches up to 10–15 %.

DOI: 10.1103/PhysRevA.76.032511 PACS number(s): 33.70.Ca, 33.50.Hv

I. INTRODUCTION

Heteronuclear alkali-metal dimers are offering a number of new possibilities in forming and employing the ultracold molecules. Owing to their permanent electric dipole moment, collision processes, including chemical reactions, can be manipulated and controlled at ultralow temperature conditions by electric fields. In particular, the NaCs molecule is of special interest because of its large permanent electric dipole moment values of $d(R_e)=4.6$ D for the ground X $^1\Sigma^+$ state as compared, say, to KRb (around 0.6 D) or RbCs (around 1.2 D) [1,2]. The experimental studies of inelastic cold collisions in a Na-Cs trap were reported in Ref. [3]. The first successful formation of translationally cold NaCs molecules by photoassociation in a laser-cooled atomic vapor of Na and Cs atoms was realized in Refs. [4,5], where the ultracold NaCs molecule formation rate was measured and compared with theoretical prediction. In particular, the low-lying $^1\Pi$ states of NaCs are of interest since photoassociation of the cold colliding atoms via the intermediate spin-orbit coupled $^1\Pi \sim {}^3\Sigma^+ \sim {}^3\Pi \sim {}^1\Sigma^+$ states might occur preferable (according, for instance, to calculations for LiH [6,7]). Since the cooling experiments usually include radiative absorption and decay cycles, the information on radiative lifetimes of excited electronic states and transition probabilities is required to reliably estimate the outcome and to select an optimal transition cycle.

From more general viewpoint, measurements of radiative lifetimes and evaluation of transition probabilities are of interest with regard to a detailed insight into molecular structure. Indeed, transition dipole moments derived from the computed wave functions of upper and lower states are much more sensitive to approximation errors of these functions than are the energies of those states. Experimentally determined radiative characteristics such as radiative lifetimes and transition intensities are therefore well suited to test the quality of calculated wave functions [8]. A comparison between measured and calculated radiative characteristics allows one improving theoretical models used in all-electronic calculations.

To achieve this goal, it is necessary to select an excited state in the NaCs molecule with no pronounced perturbation effects. This became possible due to recent progresses in energy properties studies of NaCs, both experimental [9–12] and theoretical [13–15]. As far as experimental spectroscopic information is concerned, the extensive set of Dunham coefficients and a corresponding Rydberg-Klein-Rees (RKR) potential energy curve (PEC) valid up to $v'' \leqslant 64$ of the ground electronic state X $^1\Sigma^+$ was first obtained in Ref. [16] by use of Doppler-free polarization spectroscopy in combination with double-resonance techniques and laser-induced fluorescence (LIF) spectroscopy. Then, the refined empirical X $^1\Sigma^+$ inverted perturbation approach (IPA) PEC up to dissociation limit was obtained in Ref. [9] by means of Fourier transform spectroscopy (FTS) analysis of LIF spectra of the (1–3) $^1\Pi$-X $^1\Sigma^+$ and (4)E $^1\Sigma^+$-X $^1\Sigma^+$ electronic transitions. The highly accurate analytical and pointwise PECs of both X $^1\Sigma^+$ and a $^3\Sigma^+$ electronic states converging to the lowest Na(3S)+Cs(6S) asymptote were derived in Ref. [10] using coupled-channels calculations which yield correct asymptotic behavior and a reliable description of cold collisions between Na and Cs atoms as well as a prediction of

scattering lengths and Feshbach resonances. The accurate empirical IPA PEC of the excited (3) $^1\Pi$ state corresponding to 95% of the potential well depth is presented in Ref. [11], while the moderate accurate pointwise PEC of the $B(1)$ $^1\Pi$ state is constructed in Ref. [12]. The effective Dunham coefficients valid for the lowest $v'=0$, 1, and 2 vibrational levels of the perturbed $D(2)$ $^1\Pi$ state are given in Ref. [16].

Regarding the available theoretical results, the *ab initio* PECs for the lowest 32 electronic states of NaCs were calculated in Ref. [13] over a wide range of internuclear distance; in Ref. [14] the PECs are calculated accounting for spin-orbit effects. This calculation is based on nonempirical core polarization pseudopotential (CPP) and full configuration interaction methods correlating two valence electrons. Recently, the nonrelativistic PECs, permanent and transition dipole moments for the ground and excited states of mixed alkali dimers (including NaCs) were evaluated in Refs. [2,15] by a similar CPP approach using, however, a very extensive Gaussian basis set for two valence electrons.

Electric permanent dipole moments $d(v',J')$ and Λ splitting (q factors) in the (3) $^1\Pi$ state of the NaCs molecule were measured over a wide range of vibrational $v' \in [0,34]$ quantum numbers using the combination of dc Stark mixing and electric radio frequency-optical double resonance methods [17]. The experimental results were supported by quasirelativistic many-body multipartitioning perturbation theory (MPPT) electronic structure calculations on adiabatic PECs, permanent electric dipoles and angular coupling matrix elements for the (1–3) $^1\Pi$ states [17]. Both experimental and theoretical data proved high d values of 5–8 D for the (3) $^1\Pi$ state and smaller d values of around 1 D for the $D(2)$ $^1\Pi$ state ($v' \leqslant 2$).

As follows from the above discussion, at present there are no experimental data on radiative properties of NaCs. At the same time the existing spectroscopic information yielding unambiguous assignment of the NaCs rovibronic levels made it possible to extend our previous experience of studying the radiative properties of mixed alkali dimers, such as NaK [18] and NaRb [19–21], in order to perform similar investigations in NaCs. Thus, the main goal of the present paper is to provide experimental radiative lifetimes of the (3) $^1\Pi$ and $D(2)$ $^1\Pi$ states of the NaCs molecule, with an emphasize on the (3) $^1\Pi$ state which is free from perturbation effects [11]. In addition, the relevant quenching collision cross sections with Cs atoms (2,3) $^1\Pi$ NaCs+Cs are provided. The direct measurements are accompanied by the radiative lifetime calculations performed for particular rovibronic levels of the low-lying (1–3) $^1\Pi$ states in the framework of a pure **a** Hund's coupling case by means of the approximate sum rule over the lower-lying vibronic states [22,23] and *ab initio* (present MPPT and previous CPP [15]) electronic transition dipole moment functions. Propagation of the systematic errors of *ab initio* transition moments and potential energy curves into the resulting lifetime estimates is analyzed as well.

II. LIFETIME MEASUREMENTS

A. Experimental setup

The experimental setup was the same as used before in Refs. [20,21] for the NaRb lifetime measurements. The NaCs molecules were produced in a thermal cell from alkali-resistant glass by heating a mixture of cesium and sodium metals in an approximate proportion 1:1 by weight. Before the experiments the cell was degassed at 400 °C, then filled under vacuum with the metals by distillation, and sealed off. During the measurements the oven temperature was kept within 180–280 °C. To induce the (3) $^1\Pi \rightarrow X\,^1\Sigma^+$ fluorescence, see Fig. 1, four Ar^+ laser (Spectra Physics 171, with intracavity etalon) lines with fixed wavelength 514.5, 496.5, 487.9, and 476.5 nm were used. A tunable single mode ring dye laser (Coherent CR 699-21) with Rhodamin 6G dye was used to excite the $D\,^1\Pi \rightarrow X\,^1\Sigma^+$ transition fluorescence. LIF was detected at right angles to the incident laser beam and dispersed by a DFS-12 double monochromator having reciprocal dispersion of 0.5 nm/mm and providing spectral resolution about 0.02 nm at reasonable slit widths.

The LIF kinetic measurements were performed on the particular fluorescence lines singled out by the monochromator of the LIF progression originating from a selected excited $v'(J')$ level of the (2,3) $^1\Pi$ state. The appropriate spectral region free of alien fluorescence lines of other origin was chosen. The laser beam was modulated by a ML-102 electrooptical modulator (DKDP crystal) at 850 kHz repetition rate. The laser pulse parameters, see Fig. 2(a), dashed line, were the following: pulse width about 100 ns, rear front about 20 ns, and modulation depth better than 1:50. At kinetic measurements the monochromator slits were kept at 0.5–1 mm width in order to provide a measurable fluorescence signal. The scattered laser light was cut off with colored glass filters placed before the entrance slit. At these conditions the LIF response detected with a photomultiplier tube (PMT) in photon counting regime did not exceed 3000 counts/s. One-photon pulses from PMT were discriminated, amplified and formed to standard (1 V, 10 ns duration) pulses by fast electronics. The LIF decay curves were recorded by time-correlated single-photon counting technique with a time-amplitude convertor (TAC) and a multichannel amplitude analyzer (MCA). Time resolution of the system was determined as 1.35 ns/channel by calibration with about 1% accuracy. The TAC was operated in the inverse start-stop regime. It means that the one-photon pulses from PMT were used to start the TAC, whereas the stop pulses came at 850 kHz frequency from the nanosecond generator synchronized with the laser modulation unit.

B. Rovibrational $v'(J')$ assignment of the (3) $^1\Pi$ and $D(2)$ $^1\Pi$ levels

The calculated [13] potential energy curves of the electronic states of NaCs relevant to the present study are shown in Fig. 1. Recent Fourier transform analysis of the (1–3) $^1\Pi \rightarrow X\,^1\Sigma^+$ NaCs transitions in LIF performed in Refs. [9–11] greatly facilitated the choice and assignment of the desired $v'(J')$ levels under study. For kinetic measurements, the strongest and spectrally cleanest (3) $^1\Pi \rightarrow X\,^1\Sigma^+$ fluorescence lines originating from five (3) $^1\Pi(v' \in [3,25])$ levels (Table I) were selected from a numerous (3) $^1\Pi \rightarrow X\,^1\Sigma^+$ transitions excited by an Ar^+ laser, see, for example, EPAPS in Ref. [11]. In the present experiment,

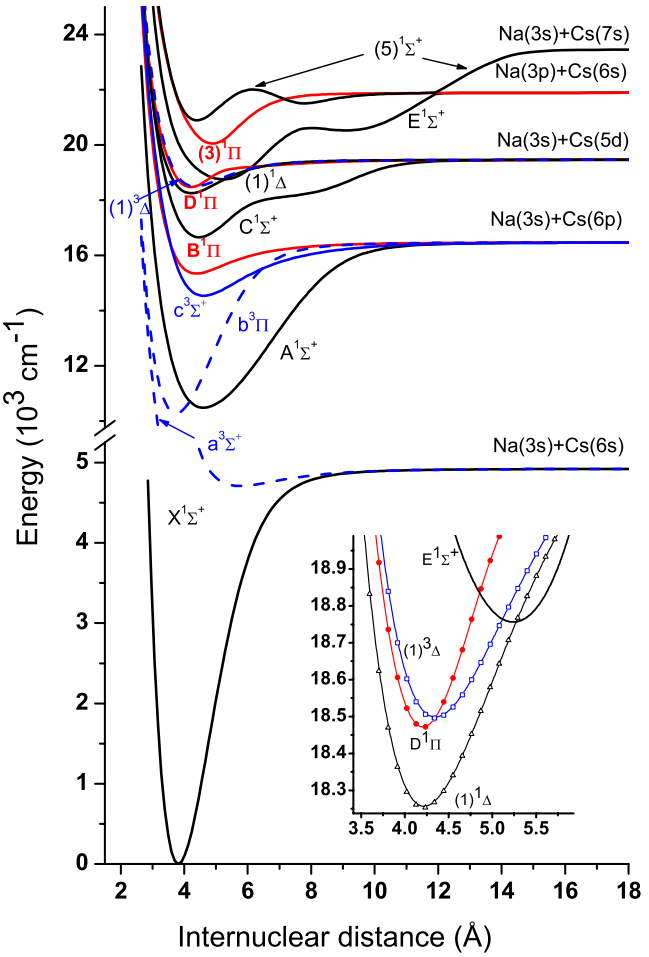

FIG. 1. (Color online) Schema of potential energy curves (PECs) for the low-lying singlet states of NaCs molecule borrowed from Ref. [13]. The triplet states are hidden [except for the lowest $a\ ^3\Sigma^+$, $b\ ^3\Pi$, $c\ ^3\Sigma^+$, and (1) $^3\Delta$ states] to simplify the picture while the insert enlarges the region near the locally perturbed $D(2)\ ^1\Pi$ state.

first, the characteristic fragments of the $(2,3)\ ^1\Pi \rightarrow X\ ^1\Sigma^+$ progressions were recorded simultaneously with Ne discharge spectral lines, thus ensuring the calibration of LIF

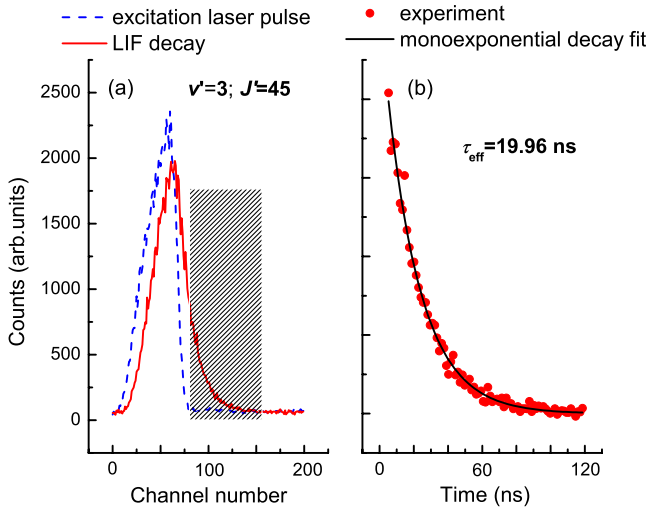

FIG. 2. (Color online) Example of laser pulse and fluorescence decay kinetic signals. (a) Excitation pulse and LIF response. (b) LIF decay monoexponential fit for the NaCs (3) $^1\Pi$ ($v'=3, J'=45$) level. The shaded area marks the decay region used for τ evaluation.

spectra with absolute wavelength accuracy about 0.05 nm. Second, the recorded spectra fragments were compared with Fourier transform spectra that allowed us to perform unambiguous assignment of the (3) $^1\Pi(v',J')$ levels. The $D(2)\ ^1\Pi \leftarrow X\ ^1\Sigma^+$ excitation frequency needed to excite the desired $D(2)\ ^1\Pi(v',J')$ level was calculated using the empirical PEC for the ground state [9] and Dunham coefficients for the upper state [16].

C. Kinetic signal processing and extrapolation to a zero pressure

A typical laser pulse and a LIF decay curve are presented in Fig. 2(a). The shaded area in Fig. 2(a) marks the decay region used for τ evaluation. The beginning and the end of the latter are determined by the respective time instants when the laser pulse and LIF intensity drop to the background level. Least square analysis proved that LIF decay from a

TABLE I. The experimental radiative lifetimes τ_i^{rad} and effective collision cross sections σ_i for the (3) $^1\Pi$ and $D(2)\ ^1\Pi$ states of the NaCs molecule excited in a $v'(J') \leftarrow v''(J'')$ transition by a fixed Ar^+ (λ_{exc}) and tunable Rhodamin 6G dye (ν_{exc}) laser lines, respectively.

λ_{exc}, nm	$v'(J')$	$v''(J'')$	τ_i^{rad} (ns)	$\sigma_i(10^{-14}$ cm$^2)$
			(3) $^1\Pi$ state	
514.5	3(45)	7(45)	29.15±0.96	4.6±0.5
514.5	3(106)	5(106)	25.27±2.08	3.6±1.3
496.5	8(25)	3(24)	27.40±0.74	2.9±0.2
488.0	17(47)	4(47)	23.56±0.60	4.9±0.6
476.5	25(67)	2(68)	20.82±0.38	1.5±0.3
ν_{exc} (cm^{-1})			$D(2)\ ^1\Pi$ state	
17557.77	0(16/24)[a]	7(16/23)	36.9±1.13	3.8±0.3

[a]Measured on two overlapping lines with $J'=16$ and 24, with around 75% of LIF intensity for $J'=16$.

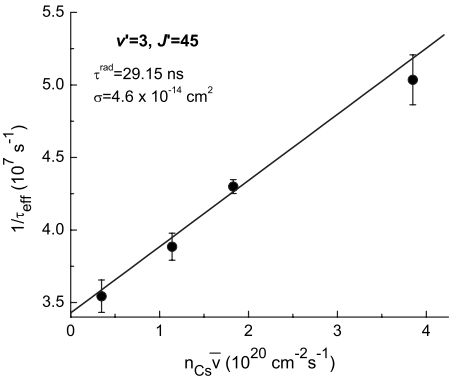

FIG. 3. Stern-Volmer plot of the inverse effective lifetime $(\tau_i^{\text{eff}})^{-1}$ for the NaCs (3) $^1\Pi$ $(v'=3;J'=45)$ level as dependent on the product of Cs atom concentration n_{Cs} and mean relative velocity $\bar{v}$ of the colliding partners, see Eq. (1).

selectively excited $v'(J')$ level was monoexponential. Figure 2(b) presents an example of the monoexponential fit of LIF decay from the (3) $^1\Pi(v'=3,J'=45)$ level. Data processing of LIF decay curves yielded the reciprocal effective lifetime $1/\tau_i^{\text{eff}}$ of the rovibronic level i at particular temperature T, whereas collision free lifetimes τ_i^{rad} were obtained by varying the temperature within the 180–280 °C range and extrapolating to a zero concentration n_{Cs} of Cs atoms, see Fig. 3, according to the Stern-Volmer rule

$$\frac{1}{\tau_i^{\text{eff}}} = \frac{1}{\tau_i^{\text{rad}}} + n_{\text{Cs}}\sigma_i\bar{v}, \tag{1}$$

where σ_i is the effective collisional quenching cross section and $\bar{v}=\sqrt{8kT/\mu}$ is the mean relative velocity of the colliding partners assuming Maxwellian velocity distribution (μ: reduced mass of colliding partners, k: Boltzman constant). The population quenching of the NaCs $^1\Pi(v',J')$ rovibronic levels by Cs atoms was considered as a dominating collision process since n_{Cs} is expected to be about two orders of magnitude higher than the concentration of Na, Na_2, and Cs_2 [24]. A possible systematic inaccuracy in measuring concentration is estimated as around 10% yielding less than 0.5% additional error of measured lifetime values. The resulting experimental radiative lifetimes τ_i^{rad} and collision cross sections σ_i for the (3) $^1\Pi$ and $D(2)$ $^1\Pi$ levels of the NaCs molecule are presented in Table I. The uncertainties in τ_i^{rad} values include statistical errors with 0.95 confident limit estimated from several measurement series as well as a contribution from the Cs atom concentration uncertainty. The possible influence of flight-out-of-view effect of excited NaCs molecules [25] on the τ_i^{rad} values could be neglected since at laser beam width $a\approx 1$ mm the ratio $\bar{v}/a\approx 2\times 10^4$ s^{-1} is considerably smaller than the $1/\tau_i^{\text{eff}}\approx 3\times 10^7$ s^{-1} value.

III. LIFETIME CALCULATIONS

Though radiative lifetime τ_i^{rad} is a property of a single excited level i, inverse lifetime being the rate at which the population of level i exponentially decays, τ_i^{rad} has to be described via transition probabilities between A_i^j the levels $i\rightarrow j$. In particular, the radiative lifetime for the rovibronic $v'(J')$ levels of an electronically excited level $i\in(1-3)$ $^1\Pi$ states was defined as the summation over the spontaneous emission Einstein coefficients $A_{iv'J'}^{jv''J''}$ [8] for bound and embedding continuum lower-lying $v''(J'')$ rovibronic states (see Fig. 1):

$$\frac{1}{\tau_i^{\text{rad}}} = \sum_j \sum_{v''} \sum_{J''} A_{iv'J'}^{jv''J''}$$

$$A_{iv'J'}^{jv''J''} = \frac{8\pi^2}{3\hbar\epsilon_0}(\nu_{iv'J'}^{jv''J''})^3 |\langle v_i'(J')|d_{ij}|v_j''(J'')\rangle|^2 \frac{S_{J'J''}}{2J'+1}, \tag{2}$$

where $\nu_{iv'J'}^{jv''J''}=E_i^{v'J'}-E_j^{v''J''}$ is the transition wavenumber, $S_{J'J''}$ is Hönl-London factor, $d_{ij}(R)$ is the electric dipole transition moment, $E^{v,J}$ and $|v(J)\rangle$ are the respective rovibronic energies and rovibrational wave functions of the upper (i) and lower (j) states. To avoid tedious explicit summation and integration over the lower-lying vibrational states, the present τ_i^{rad} values were estimated by means of the approximate sum rule [22,23]

$$\frac{1}{\tau_i^{\text{rad}}} \approx \frac{8\pi^2}{3\hbar\epsilon_0}\langle v_i'(J')|\left[\sum_j \Delta U_{ij}^3 d_{ij}^2\right]|v_i'(J')\rangle, \tag{3}$$

where the $\Delta U_{ij}(R)=U_i(R)-U_j(R)$ are the differences between the corresponding adiabatic PECs. The expectation value defined by the relation (3) can be considered, from practical viewpoint, an accurate analog of the direct sum (2) since the relative error of the approximation has been proved not to be exceed 1% for strong electronic transitions [26].

The required *ab initio* electric dipole transition moment functions $d_{ij}^{ab}(R)$ and the differences of potentials $\Delta U_{ij}^{ab}(R)$ between (1–3) $^1\Pi$ and lower-lying singlet states were calculated at internuclear distances $R\in[3.0,9.5]$ Å by many body multipartitioning perturbation theory (MPPT) correlating 18 electrons explicitly [17]. The spin-independent relativistic effects were taken into account via replacing the inner atomic core of Cs atom by the spin-averaged shape-consistent relativistic pseudopotential [27]. Electronic energies and valence wave functions were obtained from the state-selective effective Hamiltonian constructed in the full valence (two-electron) configuration interaction space; the core-valence correlation and residual core polarization effects were incorporated through perturbative evaluation of effective valence-shell interactions at the second order. The resulting transition matrix elements given in Table II were derived from one-particle spin-free transition density matrices computed at the first MPPT order [28]. The $d_{ij}^{\text{MPPT}}(R)$ functions and their CPP counterparts $d_{ij}^{\text{CPP}}(R)$ [15] used for the present lifetime estimates are depicted in Fig. 4.

The nonadiabatic spin-orbit coupling (SOC) effect between singlet and triplet states of NaCs dimer has been completely neglected at the present treatment and, hence, only the spin-allowed (1–3) $^1\Pi\rightarrow{}^1\Lambda$ transitions have been accounted in the sum of Eq. (3). Furthermore, the direct summation $\Sigma_j[\Delta U_{ij}^{ab}]^3[d_{ij}^{ab}]^2$ in Eq. (3) highlights that the life-

TABLE II. The MPPT transition dipole moments as a function of internuclear distance R. All values are given in atomic units.

R	$B\ ^1\Pi - X\ ^1\Sigma^+$	$D\ ^1\Pi - X\ ^1\Sigma^+$	$(3)\ ^1\Pi - X\ ^1\Sigma^+$	$D\ ^1\Pi - A\ ^1\Sigma^+$	$D\ ^1\Pi - B\ ^1\Pi$
5.6	3.164	−0.158	0.754	1.968	1.618
6.0	3.150	−0.363	0.715	2.004	2.187
6.4	3.113	−0.686	0.673	2.049	2.551
6.8	3.075	−0.923	0.646	2.079	2.805
7.2	3.037	−1.121	0.652	2.081	2.965
7.6	2.999	−1.287	0.692	2.065	3.045
8.0	2.959	−1.430	0.772	2.034	3.062
8.4	2.913	−1.544	0.904	2.013	3.052
8.7	2.881	−1.594	1.037	2.005	3.040
9.0	2.852	−1.601	1.210	2.009	3.044
9.5	2.811	−1.474	1.585	2.043	3.117
10.0	2.785	−1.132	1.997	2.070	3.229
11.0	2.773	−0.359	2.472	2.021	3.269
12.0	2.790	0.051	2.627	1.978	3.202
13.0	2.822	0.233	2.685	1.972	3.126
14.0	2.861	0.295	2.702	2.026	3.072
16.0	2.938	0.276	2.691	2.277	2.991
18.0	3.002	0.202	2.660	2.549	2.935

times of the $B\ ^1\Pi$ and $(3)\ ^1\Pi$ states are mainly determined by a single transition to the ground $X\ ^1\Sigma^+$ state while the contribution of the additional $D\ ^1\Pi \rightarrow A\ ^1\Sigma^+$ decay channel is significant for the $\tau^{\mathrm{rad}}_{D^1\Pi}$ values. Indeed, the relative contribution of the additional B, $(3)\ ^1\Pi \rightarrow {}^1\Lambda$ electronic transitions into $\tau^{\mathrm{rad}}_{B,(3)^1\Pi}$ values does not exceed 1% while the contribution of the $D\ ^1\Pi \rightarrow A\ ^1\Sigma^+$ transition into $\tau^{\mathrm{rad}}_{D^1\Pi}$ values reaches up to 10–15 %.

IV. DISCUSSION AND CONCLUSIONS

The calculated radiative lifetimes for the rovibronic $(J'=1)$ levels of the (1–3) $^1\Pi$ states are depicted in Fig. 5 together with the atomic lifetimes related to the Na(3 ^{2}S) +Cs(6 ^{2}P), Na(3 ^{2}S)+Cs(5 ^{2}D) and Na(3 ^{2}P)+Cs(6 ^{2}S) dissociation limits of the $B(1)\ ^1\Pi$, $D(2)\ ^1\Pi$, and $(3)\ ^1\Pi$ states, respectively (see Fig. 1). The vibrational wavefunctions $|v_i'(J')\rangle$ required for the upper (1–3) $^1\Pi$ states were evaluated in the framework of standard adiabatic approximation [8] using three different kinds of available PECs, namely, the empirical $U_i^{\mathrm{emp}}(R)$, the *ab initio* $U_i^{ab}(R)$, and the so-called "difference-based" PEC: $U_i^{\mathrm{dif}}(R) = U_X^{\mathrm{emp}}(R) + [U_i^{ab}(R) - U_X^{ab}(R)]$, see, e.g., Ref. [28], where $U_X^{\mathrm{emp}}(R)$ is the empirical IPA potential for the ground $X\ ^1\Sigma^+$ state [10].

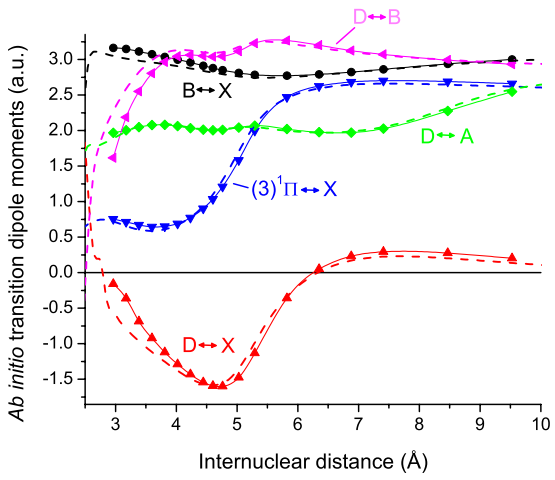

FIG. 4. (Color online) MPPT (solid lines) and CPP (dash lines) [15] $B,D,(3)\ ^1\Pi$-$X\ ^1\Sigma^+$, $D\ ^1\Pi$-$A\ ^1\Sigma^+$ and $D\ ^1\Pi$-$B\ ^1\Pi$ transition dipole moments for the NaCs molecule.

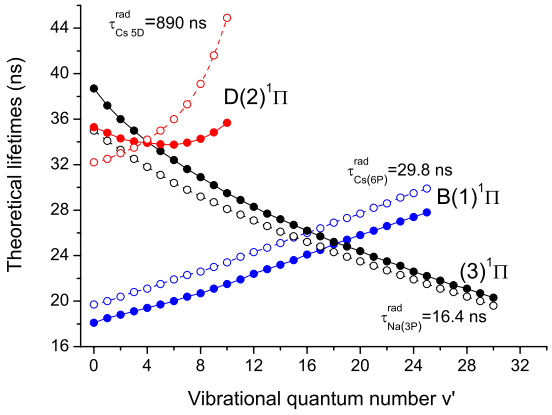

FIG. 5. (Color online) The radiative lifetimes of the NaCs (1–3) $^1\Pi(J'=1)$ states predicted by Eq. (3) using MPPT (closed circles) and CPP (open circles) [15] transition dipole moments $d_{ij}^{ab}(R)$, and corresponding $\Delta U_{ij}^{ab}(R)$ functions. The vibrational upper state wavefunctions were calculated by the relevant "difference-based" PECs $U_i^{\mathrm{dif}}(R)$.

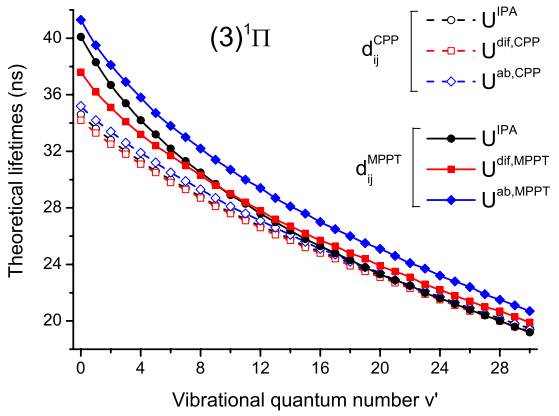

FIG. 6. (Color online) Radiative lifetime estimates $\tau^{\mathrm{rad}}_{(3)\,^1\Pi}(J'=50)$ obtained by the relevant MPPT (closed symbols) and CPP (open symbols) [15] functions, respectively.

As can be seen from Fig. 5, the calculated radiative lifetimes $\tau^{\mathrm{rad}}_{(3)\,^1\Pi}(v')$ of the (3) $^1\Pi$ state monotonically decrease towards the atomic lifetime value $\tau^{\mathrm{rad}}_{\mathrm{Na}(3\,^2\mathrm{P})}=16.4$ ns [29] as the vibrational quantum number v' increases whereas the $\tau^{\mathrm{rad}}_{B\,^1\Pi}(v')$ values monotonically increase towards the atomic value $\tau^{\mathrm{rad}}_{\mathrm{Cs}(6\,^2\mathrm{P})}=29.8$ ns [29]. The predicted MPPT and CPP $\tau^{\mathrm{rad}}_{D\,^1\Pi}(v')$ is expected to increase steeply with v' to reach the atomic lifetime $\tau^{\mathrm{rad}}_{\mathrm{Cs}(5\,^2D)}=890$ ns [29] at the dissociation limit.

It is worth noting that in the $D(2)\,^1\Pi$ state case the MPPT and CPP calculations demonstrate a very different behavior in the $v'=0$ to 10 range (see Fig. 5). Indeed, while the MPPT $\tau^{\mathrm{rad}}_{D\,^1\Pi}(v')$ curve shows no pronounced v' dependence, the CCP curve demonstrates a rather steep growth of about 30%. This might be connected with the difference in the steep R dependence of the D-X transition dipole moment function $d(R)$ around equilibrium internuclear distances, see Fig. 4. Thus, the propagation of the inaccuracies of the relevant $d^{\mathrm{MPPT}}(R)$ and $d^{\mathrm{CPP}}(R)$ functions into radiative lifetimes could be more pronounced for the $D(2)\,^1\Pi$ state. It should be mentioned that it is not worth presenting $\tau^{\mathrm{rad}}_{D\,^1\Pi}(v')$ adiabatic estimates for larger v's since they are expected to be influenced by rather strong nonadiabatic state mixing. On the contrary, the (3) $^1\Pi$ state as being almost not affected by perturbations, allows more reliable testing of theoretical approaches.

Figure 6 demonstrates the influence of the particular selected $U_{(3)\,^1\Pi}(R)$ PEC and $d_{(3)\,^1\Pi-X\,^1\Sigma^+}(R)$ transition moments on the $\tau^{\mathrm{rad}}_{(3)\,^1\Pi}(v')$ values predicted for the $J'=50$ levels of the (3) $^1\Pi$ state. The divergence of calculated $\tau^{\mathrm{rad}}_{(3)\,^1\Pi}$ values is most pronounced for small v' and the lifetimes calculated with the relevant CPP functions are less dependent on the choice of the particular PEC. One may conclude that the MPPT-based estimates are exhibiting more pronounced dependence on the exploited PECs. It is important that the usage of "difference-based" PEC discussed above allows one to obtain almost the same lifetime estimates as with the empirical PEC.

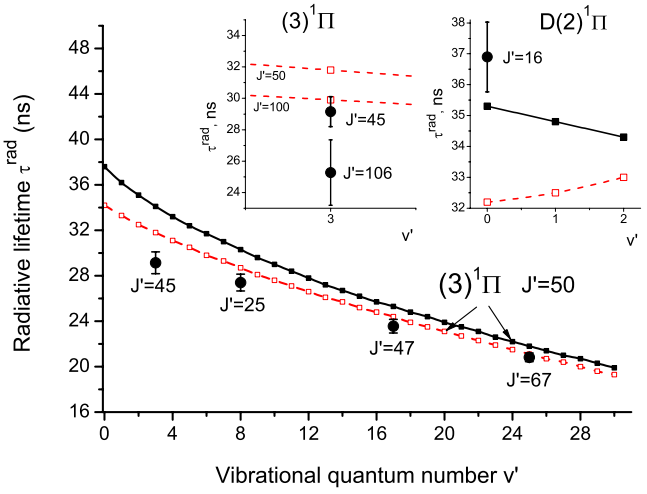

FIG. 7. (Color online) Comparison of the experimental radiative lifetimes of the NaCs (3) $^1\Pi$ and $D(2)\,^1\Pi$ states with their theoretical counterparts calculated by Eq. (3) using the *ab initio* MPPT (solid lines) and CPP (dashed lines) transition moments $d^{ab}_{ij}(R)$ and potential differences $\Delta U^{ab}_{ij}(R)$. The required vibrational wave functions of the upper states $|v'_i(J')\rangle$ were computed using the corresponding MPPT and CPP "difference-based" $U^{\mathrm{dif}}_i(R)$ PECs.

A comparison of measured and calculated lifetimes for the (3) $^1\Pi$ and $D(2)\,^1\Pi$ states of NaCs is presented in Fig. 7. The calculated τ values demonstrate rather sufficient agreement with their measured counterparts, though systematically overestimating the latter, coming closer to the measured values for higher v's. However, the discrepancy of around 8% even with respect to the closest τ^{CPP} value still remains for $v'=3$. The theory predicts a weak systematic decrease of the $\tau^{\mathrm{rad}}_{(3)\,^1\Pi}(J')$ values with rotation; though being small for J' below 50, a more pronounced decrease up to 2 ns is predicted as J' changes from 50 to 100, see left inset in Fig. 7. The experimental τ^{rad} values for $v'=3$ measured at two different $J'=45$ and 106 support this prediction.

Regarding the $D(2)\,^1\Pi$ state, both CPP- and MPPT-based calculations underestimate the measured $\tau^{\mathrm{rad}}_{D\,^1\Pi}$ value for $v'=0$, $J'=16$, the MPPT calculation being closer to the experiment, see the right inset in Fig. 7. Such a discrepancy can be attributed to the spin-orbit coupling of the $D(2)\,^1\Pi$ state with the close-lying metastable (1) $^3\Delta$ state (see Fig. 1) which is ignored in the calculations. Indeed, even a weak SOC effect between the upper states having essentially different adiabatic (unperturbed) lifetimes can affect the radiative lifetimes of the particular rovibronic levels of the mutually perturbed states significantly [8]. At the same time, the recent investigation of the lifetimes of the $C\,^1\Sigma^+$ state of the NaRb molecule [21] proved that even a strong SOC of the lower-lying $A\,^1\Sigma^+$ and $b\,^3\Pi$ states does not affect the upper $C\,^1\Sigma^+$ state lifetimes, though leading to a pronounced relative intensity redistribution in the corresponding rovibronic $C\rightarrow A\sim b$ transitions [30].

As follows from the above analysis, the closest to the experimental values theoretical lifetime estimates for both $D(2)\,^1\Pi$ and (3) $^1\Pi$ states were obtained with the

"difference-based" potentials $U_i^{\mathrm{dif}}(R)$. This is more significant for the MPPT results which suffer from the systematic R-dependent errors to a greater extent than their CPP counterparts. Nevertheless, the main part of the observed discrepancy between theoretical and experimental lifetimes can be most likely ascribed to the uncertainty in the *ab initio* transition dipole moments in spite of a visual impression (see Fig. 4) that the $d_{ij}^{\mathrm{MPPT}}(R)$ and $d_{ij}^{\mathrm{CPP}}(R)$ functions look very similar to each other for most transitions. In fact, the deviation of the calculated $d_{ij}^{\mathrm{MPPT}}(R)$ moments from their $d_{ij}^{\mathrm{CPP}}(R)$ counterparts can reach up to 5–10 % for particular (basically small) internuclear distances. This uncertainty can easily propagate into the 10–20 % difference between the MPPT and CPP lifetime estimates.

Finally, it makes sense to compare the present NaCs (3) $^1\Pi$ state radiative lifetimes with the lifetimes of NaK and NaRb mixed alkali-metal dimers in their $D(2)\ ^1\Pi$ state dissociating to the respective Na($3p$)+K($4s$) and Na($3p$)+Rb($5s$) limits. As was determined by measurements and theoretical estimates, the radiative (2) $^1\Pi(v';J')$ lifetimes for both NaK [18] and NaRb [19,20] molecules drop from 22 to 16 ns with v' increasing, τ^{rad} rapidly coming close to the Na($3p$) atom lifetime. It can be seen from Figs. 5–7 that the spontaneous lifetimes of the (3) $^1\Pi$ NaCs $v'(J')$ states exhibit larger values and a slower decrease from 32 to 20 ns for $v'=3-25$. This is caused by a different behavior of the corresponding $d_{^1\Pi-X\ ^1\Sigma^+}(R)$ functions. Indeed, the NaCs $d_{(3)\ ^1\Pi-X\ ^1\Sigma^+}(R)$ moment, prior to growth, exhibits a slight decrease within the $R=3-4$ Å range (see Fig. 4) in contrast to a monotonous increase of NaK [18] and NaRb [19] $d_{D\ ^1\Pi-X\ ^1\Sigma^+}(R)$ function within $R=3-6$ Å range. The effective cross sections σ for quenching collisions of NaCs in the $(2,3)\ ^1\Pi$ states with Cs atoms, see Table I, do not differ much from the cross sections of (2) $^1\Pi$ NaRb with Rb atoms being within $(2.5-6.2)\times 10^{-14}$ cm^2 [20,21].

ACKNOWLEDGMENTS

The authors are indebted to M. Aymar and O. Dulieu for providing the CPP potential energy curves and transition dipole moment functions of NaCs dimer prior to their publication, as well as to M. Auzinsh for numerous useful discussions. This work has been supported by the NATO SfP-978029 Optical Field Mapping grant. Riga team is grateful for the support by the Latvian Science Council Grant No. 04.1308. The Moscow team is grateful for the support from the Russian Foundation for Basic Researches (Grants Nos. 06-03-32330 and 06-03-32346). J.Z. is grateful for the support from the European Social Fund.

[1] P. J. Dagdigan and L. Wharton, J. Chem. Phys. **57**, 1487 (1973).
[2] M. Aymar and O. Dulieu, J. Chem. Phys. **122**, 204302 (2005).
[3] J. P. Shaffer, W. Chalupczak, and N. P. Bigelow, Phys. Rev. A **61**, 011404(R) (1999).
[4] C. Haimberger, J. Kleinert, M. Bhattacharya, and N. P. Bigelow, Phys. Rev. A **70**, 021402(R) (2004).
[5] C. Haimberger, J. Kleinert, O. Dulieu, and N. P. Bigelow, J. Phys. B **39**, S957 (2006).
[6] E. Taylor-Juarros, R. Cote, and K. Kirby, Eur. Phys. J. D **31**, 213 (2004).
[7] E. Juarros, K. Kirby, and R. Cote, J. Phys. B **39**, S965 (2006).
[8] H. Lefebvre-Brion and R. W. Field, *The Spectra and Dynamics of Diatomic Molecules* (Academic Press, New York, 2004).
[9] O. Docenko, M. Tamanis, R. Ferber, A. Pashov, H. Knöckel, and E. Tiemann, Eur. Phys. J. D **31**, 205 (2004).
[10] O. Docenko, J. Zaharova, M. Tamanis, R. Ferber, A. Pashov, H. Knöckel, and E. Tiemann, J. Phys. B **39**, S929 (2006).
[11] O. Docenko, M. Tamanis, J. Zaharova, and R. Ferber, A. Pashov, H. Knöckel, and E. Tiemann, J. Chem. Phys. **124**, 174310 (2006).
[12] J. Zaharova, O. Docenko, M. Tamanis, R. Ferber, A. Pashov, H. Knöckel, and E. Tiemann, J. Chem. Phys. (to be published).
[13] M. Korek, A. R. Allouche, K. Fakhreddine, and A. Chaalan, Can. J. Phys. **78**, 977 (2000).
[14] M. Korek, S. Bleik, and A. R. Alouche, J. Chem. Phys. **126**, 124313 (2007).
[15] M. Aymar and O. Dulieu, Mol. Phys. (to be published).
[16] U. Diemer, H. Weickenmeier, M. Wahl, and W. Demtröder, Chem. Phys. Lett. **104**, 489 (1984).
[17] J. Zaharova, O. Nikolayeva, M. Tamanis, M. Auzinsh, R. Ferber, A. Zaitsevskii, E. A. Pazyuk, and A. V. Stolyarov, J. Chem. Phys. **124**, 184318 (2006).
[18] M. Tamanis, M. Auzinsh, I. Klincare, O. Nikolayeva, R. Ferber, A. Zaitsevskii, E. A. Pazyuk, and A. V. Stolyarov, J. Chem. Phys. **109**, 6725 (1998).
[19] A. Zaitsevskii, S. O. Adamson, E. A. Pazyuk, A. V. Stolyarov, O. Nikolayeva, O. Docenko, I. Klincare, M. Auzinsh, M. Tamanis, R. Ferber, and R. Cimiraglia, Phys. Rev. A **63**, 052504 (2001).
[20] I. Klincare, M. Tamanis, and R. Ferber, Chem. Phys. Lett. **382**, 593 (2003).
[21] I. Klincare, M. Tamanis, R. Ferber, A. Zaitsevskii, E. A. Pazyuk, and A. V. Stolyarov, Eur. Phys. J. D **39**, 373 (2006).
[22] J. Tellinghuisen and P. S. Julienne, J. Chem. Phys. **81**, 5779 (1984).
[23] A. V. Stolyarov and V. I. Pupyshev, Phys. Rev. A **49**, 1693 (1994).
[24] A. N. Nesmeyanov, *Vapour Pressure of Chemical Elements* (Izdvestiya Akademii Nauk SSSR, Moscow, 1961) (in Russian).
[25] M. P. Auzinsh, M. Ya. Tamanis, R. S. Ferber, and Ya. A. Kharya, Opt. Spectrosc. **67**, 750 (1989).
[26] E. A. Pazyuk, A. V. Stolyarov, and V. I. Pupyshev, Chem. Phys. Lett. **228**, 219 (1994).
[27] R. B. Ross, J. M. Powers, T. Atashroo, and W. C. Ermler, J.

Chem. Phys. **93**, 6654 (1990).
[28] S. O. Adamson, A. Zaitsevskii, E. A. Pazyuk, A. V. Stolyarov, M. Tamanis, R. Ferber, and R. Cimiraglia, J. Chem. Phys. **113**, 8589 (2000).
[29] C. E. Theodosiou, Phys. Rev. A **30**, 2881 (1984).
[30] O. Docenko, M. Tamanis, R. Ferber, E. A. Pazyuk, A. Zaitsevskii, A. V. Stolyarov, A. Pashov, H. Knöckel, and E. Tiemann, Phys. Rev. A **75**, 042503 (2007).